



Interpolation on the Cubed Sphere with Spherical Harmonics

Jean-Baptiste Bellet, Matthieu Brachet, Jean-Pierre Croisille

► To cite this version:

Jean-Baptiste Bellet, Matthieu Brachet, Jean-Pierre Croisille. Interpolation on the Cubed Sphere with Spherical Harmonics. 2021. hal-03202236

HAL Id: hal-03202236

<https://hal.science/hal-03202236>

Preprint submitted on 19 Apr 2021

HAL is a multi-disciplinary open access archive for the deposit and dissemination of scientific research documents, whether they are published or not. The documents may come from teaching and research institutions in France or abroad, or from public or private research centers.

L'archive ouverte pluridisciplinaire **HAL**, est destinée au dépôt et à la diffusion de documents scientifiques de niveau recherche, publiés ou non, émanant des établissements d'enseignement et de recherche français ou étrangers, des laboratoires publics ou privés.

INTERPOLATION ON THE CUBED SPHERE WITH SPHERICAL HARMONICS

JEAN-BAPTISTE BELLET[†], MATTHIEU BRACHET[‡], AND JEAN-PIERRE CROISILLE[†]

ABSTRACT. We consider the Lagrange interpolation with Spherical Harmonics of data located on the equiangular Cubed Sphere. A new approach based on a suitable Echelon Form of the associated Vandermonde matrix is carried out. As an outcome, a particular subspace of Spherical Harmonics is defined. This subspace possesses a high-frequency truncation, reminiscent of the rhomboidal truncation. Numerical results show the interest of this approach in various contexts. In particular, several examples of resolution of the Poisson equation on the sphere are displayed.

1. INTRODUCTION

We consider the interpolation of data on the equiangular Cubed Sphere with Spherical Harmonics. The equiangular Cubed Sphere is a particular spherical grid widely used to discretize problems on the sphere [15]. Expanded spherical cube grids have been early considered in numerical climatology and meteorology [13, 14, 16]. The equiangular Cubed Sphere has recently served to support discrete unknowns in a variety of numerical schemes, such as finite volume schemes [18], Discontinuous Galerkin methods [12], Spectral Element methods [17] and Finite Difference schemes [3].

A more standard computational approach for PDE's on the sphere is based on the pseudospectral approximation [8]. In this case, the discrete unknowns are expanded in a finite sum of Spherical Harmonics. An important parameter of this expansion is the so-called truncation scheme, typically triangular or rhomboidal, which monitors the finite summation limit in the Spherical Harmonics series. This parameter influences both the convergence and the aliasing behaviour of the method. The discrete PDE's are then obtained by collocation at the nodes of the longitude-latitude grid. These nodes appear naturally as Gauss-Legendre quadrature nodes [1, chap. 5.7.1, p. 204]. This approach serves as the basis of many operational dynamical cores in the meteorological community. We refer to [5, 11] and the references therein.

Here we are interested by the Cubed Sphere nodes as a basic location for numerical unknowns. We wish to interpolate these unknowns with a set of “well adapted” Spherical Harmonics. By well adapted, we mean at the least, a set giving existence and uniqueness for the interpolation problem. This question seems open in the literature. Apart of its mathematical interest, this problem appears relevant from at least two points of view. First, it sheds some light on mathematical properties of the Cubed Sphere and its “approximation power” as a computational grid. Second, it could serve as a framework for defining a natural discrete harmonic analysis on the Cubed Sphere. This could lay out a pseudospectral calculus on the Sphere, different from the standard one¹.

Our first purpose is therefore to identify a suitable subspace of Spherical Harmonics having the “unisolvence” property when associated to the Cubed Sphere nodes. It turns out that this is a particular Lagrange interpolation problem. It is treated here using mainly matrix analysis. Contrary to the standard spectral case, the suggested Spherical Harmonics set entails a specific high frequency truncation. This truncation emerges as an outcome, and is not a parameter to be selected. It carries the upper frequency limit associated to a given Cubed Sphere. Second, as a byproduct of our analysis, we give an algorithm to numerically evaluate a basis of the SH subspace associated to the Cubed Sphere.

The outline is as follows. Section 2 is devoted to a brief background on the Cubed Sphere (abbrev. as CS) and the Spherical Harmonics (abbrev. as SH). The setup of the Lagrange interpolation problem (called “CS/SH”) is described in Section 3. This involves the definition of Vandermonde matrices. Theorem 9 in Section 4 is our main result. It consists in establishing a particular factorization in echelon form of the main Vandermonde matrix of the interpolation problem. An outcome is the numerical identification of a particular SH collocation subspace associated to the Cubed Sphere (Algorithm 10). Finally in Section 5, several numerical experiments and results are displayed. We show results on a set of Poisson equations on the sphere, using the pseudospectral approximation based on the preceding results.

Date: April 19, 2021.

2010 Mathematics Subject Classification. 65-41-35.

Key words and phrases. Cubed Sphere Grid, Spherical Harmonics, Spectral approximation on the sphere, Rhomboidal Truncation, Poisson equation on the sphere.

¹One of the interest of the Cubed Sphere is the isotropy and the absence of poles problem.

2. NOTATION

2.1. The equiangular Cubed Sphere. We consider the interpolation problem by Spherical Harmonics (SH) on the Cubed Sphere CS_N , $N \geq 1$ being a fixed resolution. In what follows, we assume that a Cartesian frame $\mathcal{R} = (0, i, j, k)$ is fixed. The definitions depends on this frame.

The Cubed Sphere grid CS_N is defined as the set of $6N^2 + 2$ nodes with coordinates

$$\text{CS}_N = \left\{ \frac{1}{\sqrt{1+u_l^2+u_m^2}}(\pm 1, u_l, u_m), \frac{1}{\sqrt{1+u_l^2+u_m^2}}(u_l, \pm 1, u_m), \frac{1}{\sqrt{1+u_l^2+u_m^2}}(u_l, u_m, \pm 1) \right\}, \quad (1)$$

where the u_l are equidistributed on $[-\pi/4, \pi/4]$ as

$$u_l = \tan \frac{l\pi}{2\bar{N}}. \quad (2)$$

This equidistribution justifies the name of *equiangular* Cubed Sphere. These nodes are numbered with the index $j \in \llbracket 1 : \bar{N}(N) \rrbracket$, where we denote $\bar{N}(N) = 6N^2 + 2$ (simply called \bar{N} when there is no ambiguity). Therefore,

$$\text{CS}_N = \{\mathbf{x}_j, j \in \llbracket 1 : \bar{N} \rrbracket\}. \quad (3)$$

Refer to [15] for more details and to [13] for alternative Cubed Sphere grid.

2.2. Spherical Harmonics. Our notation for Spherical Harmonic functions is as follows.

- The space Y_n is

$$Y_n = \text{Span} \{Y_n^m(\mathbf{x}), -n \leq m \leq n\}, n \geq 0, \quad (4)$$

with the SH function Y_n^m defined by

$$Y_n^m(\mathbf{x}) = (-1)^{|m|} \sqrt{\frac{(n+1/2)(n-|m|)!}{\pi(n+|m|)!}} P_n^{|m|}(\sin \theta) \times \begin{cases} \sin |m|\lambda, & m < 0, \\ \frac{1}{\sqrt{2}}, & m = 0, \\ \cos m\lambda, & m > 0. \end{cases} \quad (5)$$

We have denoted

$$\begin{cases} \mathbf{x} = (\cos \theta \cos \lambda, \cos \theta \sin \lambda, \sin \theta), \\ \lambda \in [-\pi, \pi], \text{ longitude, (or azimuth)}, \\ \theta \in [-\frac{\pi}{2}, \frac{\pi}{2}], \text{ latitude, (or elevation)}. \end{cases} \quad (6)$$

In (5), the associated Legendre function is

$$P_n^{|m|}(t) = (-1)^{|m|} (1-t^2)^{|m|/2} \frac{d^{|m|+n}}{dt^{|m|+n}} \frac{1}{2^n n!} (t^2 - 1)^n. \quad (7)$$

- We denote \mathcal{Y}_n the space of HS functions of degree less or equal to n ,

$$\mathcal{Y}_n = Y_0 \oplus \dots \oplus Y_n. \quad (8)$$

The set $(Y_n^m)_{-n \leq m \leq n}$ is an orthonormal basis of Y_n for the scalar product of $L^2(\mathbb{S}^2)$ given by

$$(f, g)_2 = \int_{\mathbb{S}^2} f(\mathbf{x})g(\mathbf{x})d\sigma. \quad (9)$$

The infinite family $(Y_n^m)_{|m| \leq n, n \in \mathbb{N}}$ is a Hilbert basis of $L^2(\mathbb{S}^2)$. We refer to [1, 9] for more details.

3. LAGRANGE INTERPOLATION ON THE CUBED SPHERE WITH SPHERICAL HARMONICS

3.1. General setup. Let $(y_j)_{1 \leq j \leq \bar{N}}$ be a set of values given at the nodes \mathbf{x}_j . We are interested in finding a SH function $p(\mathbf{x})$ satisfying the equations

$$p(\mathbf{x}_j) = y_j, \quad \forall 1 \leq j \leq \bar{N}. \quad (10)$$

Problem (CS/HS): Find an integer $N' = N'(N)$ and a subspace $\mathcal{Y}'_{N'} \subset \mathcal{Y}_{N'}$, such that the interpolation problem (10) with $p \in \mathcal{Y}'_{N'}$ has a unique solution.

Observe that the integer N' depends of N , and is part of the unknowns. In Section 4 below, we propose a constructive algorithm to solve this problem.

3.2. Vandermonde matrices. We analyse the structure of various *Vandermonde matrices* (abbreviated as VDM) associated to the problem (CS/HS).

Definition 1 (Vandermonde matrices). Let N be the resolution of the Cubed Sphere (1) and $\bar{N} = 6N^2 + 2$ the number of nodes.

- For k fixed, the rectangular matrix A_k is the VDM matrix associated to the basis $(Y_k^m)_{-k \leq m \leq k}$ of the SH space Y_k , and to the nodes $\mathbf{x}_j \in \text{CS}_N$, defined by

$$A_k \triangleq [Y_k^m(\mathbf{x}_j)]_{-k \leq m \leq k, 1 \leq j \leq \bar{N}} \in \mathbf{R}^{(2k+1) \times \bar{N}}. \quad (11)$$

- For n fixed, the matrix \mathbf{A}_n is the VDM matrix associated to the basis $(Y_k^m)_{|m| \leq k \leq n}$ of the SH space \mathcal{Y}_n . It is defined by

$$\mathbf{A}_n \triangleq \begin{bmatrix} A_0 \\ \vdots \\ A_n \end{bmatrix} \in \mathbf{R}^{(n+1)^2 \times \bar{N}}. \quad (12)$$

Remark 2. Throughout this paper, for every n , the set of indices (k, m) such that $|m| \leq k \leq n$ is sorted in lexicographic order (m is the “fast” variable). In particular, $\mathbf{A}_n = [Y_k^m(\mathbf{x}_j)]_{|m| \leq k \leq n, 1 \leq j \leq \bar{N}}$, where (k, m) is the row index.

Let N' be a fixed integer and $\mathcal{Y}_{N'} = Y_0 \oplus \cdots \oplus Y_{N'}$. Let $p(\mathbf{x})$ be the HS function with decomposition in the Legendre basis

$$p(\mathbf{x}) = \sum_{0 \leq n \leq N'} \sum_{|m| \leq n} p_n^m Y_n^m(\mathbf{x}) = [Y_n^m(\mathbf{x})]_{|m| \leq n \leq N'}^\top [p_n^m]_{|m| \leq n \leq N'}. \quad (13)$$

The vector $[p(\mathbf{x}_j)]^\top \in \mathbf{R}^{\bar{N}}$ is expressed in term of the matrix $\mathbf{A}_{N'}$ and of the vector of components $[p_n^m]$ by

$$[p(\mathbf{x}_1), \dots, p(\mathbf{x}_{\bar{N}})]^\top = \mathbf{A}_{N'}^\top [p_n^m]. \quad (14)$$

Therefore, the interpolation problem (10) is expressed with the VDM matrix $\mathbf{A}_{N'}$ by the system

$$\mathbf{A}_{N'}^\top [p_n^m] = \mathbf{y}, \quad (15)$$

where $\mathbf{y} = [y_1, \dots, y_{\bar{N}}]^\top$. A sufficient condition for the VDM matrix \mathbf{A}_n to have full rank results from the following Proposition.

Proposition 3 (Lemma 3.13 in [10]). *Let $\Omega = \{\mathbf{x}_j, 1 \leq j \leq M\} \subset \mathbb{S}^2$ be a general distribution of nodes on the 3-dimensional sphere. Let*

$$\text{sep}(\Omega) = \min_{j \neq l} \arccos(\mathbf{x}_j^\top \mathbf{x}_l) \quad (16)$$

denotes the separation distance of the nodes in Ω . Let $0 < q < \text{sep}(\Omega)$ and let $n \geq 1$ be such that $n > \frac{7.5\pi}{q}$. Then the VDM matrix

$$Z_n \in \mathbf{R}^{(n+1)^2 \times M}, \quad Z_n \triangleq [Y_k^m(\mathbf{x}_j)]_{|m| \leq k \leq n, 1 \leq j \leq M} \quad (17)$$

has full column rank M .

Remark 4. In fact, Lemma 3.13 in [10] is formulated for the d -dimensional sphere \mathbb{S}^{d-1} . Here we have $d = 3$, which is the dimension in our context.

In the particular case where the \mathbf{x}_j are the nodes of CS_N , we call $\text{sep}(\text{CS}_N)$ the separation distance on CS_N .

Corollary 5 (sufficient condition for \mathbf{A}_n to have full column rank). *Let $n \geq 1$ and let $0 < q_N < \text{sep}(\text{CS}_N)$ be such that $n > \frac{7.5\pi}{q_N}$. Then the VDM matrix $\mathbf{A}_n \in \mathbf{R}^{(n+1)^2 \times \bar{N}}$ has full column rank \bar{N} .*

Definition 6 (rank and “rank increment”). For all $n \geq 0$, the rank of \mathbf{A}_n is denoted by r_n and the rank increment between \mathbf{A}_{n-1} and \mathbf{A}_n is denoted by g_n :

$$\begin{cases} r_n \triangleq \text{rank } \mathbf{A}_n, & n \geq 0, \\ g_n \triangleq r_n - r_{n-1}, & n \geq 0, \end{cases} \quad (18)$$

with the convention $r_{-1} \triangleq 0$, $g_0 \triangleq r_0$.

By Corollary 5, for n large enough, we have $\text{rank}(\mathbf{A}_n) = \bar{N}$. This justifies the following definition.

Definition 7 (integer $N'(N)$). We call $N'(N)$ (or simply N' in case of no ambiguity), the smallest integer n such that \mathbf{A}_n has full column rank \bar{N} . Equivalently, N' is defined by

$$N' = \min\{n \geq 0 \text{ such that } r_n = \bar{N}\}. \quad (19)$$

It results from Corollary 5 that

$$\forall q_N \in (0, \text{sep}(\text{CS}_N)), \quad N' \leq \left\lceil \frac{7.5\pi}{q_N} \right\rceil, \quad (20)$$

where $\lceil \cdot \rceil$ denotes the ceil function. Refer to Remark 20 for further comments on the value $\text{sep}(\text{CS}_N)$.

4. A SPHERICAL HARMONICS COLLOCATION SET ON THE CUBED SPHERE

In this section we give a constructive algorithm to build a subspace $\mathcal{Y}'_{N'}$ of SH functions solving the problem (CS/HS) above. It consists in constructing a suitable factorization of the sequence of matrices $(\mathbf{A}_n)_{n \geq 0}$. The factorization itself will reveal both the sequence $(r_n)_{n \geq 0}$ and the integer N' in (19). See also Section 5.1 below.

4.1. Echelon form of matrices. We recall the definition of a matrix in *Column Echelon* form (abbreviated CE form).

Definition 8 (Column Echelon form). Let $A \in \mathbf{R}^{m \times n}$ be a rectangular matrix. The matrix A is said to be in CE form, if there is some $r \in \llbracket 0 : n \rrbracket$ such that

- the columns $j \in \llbracket 1 : r \rrbracket$ are nonzero, with the row index $j \in \llbracket 1 : r \rrbracket \mapsto i(j)$ of the first nonzero coefficient a non decreasing function;
- the columns $j \in \llbracket r + 1 : n \rrbracket$ are zero.

In that case, the coefficient $A(i(j), j)$, $1 \leq j \leq r$, is called the *pivot* of the column j .

A matrix $A \in \mathbf{R}^{m \times n}$ can be reduced in CE form using Gaussian elimination with partial pivoting on the columns. In addition, the number r of pivots represents the rank of the matrix.

In the sequel, we show that the VDM matrix \mathbf{A}_n in (12) can be expressed in CE form by mean of suitable orthogonal matrices.

4.2. Factorization of the VDM matrix \mathbf{A}_n . In the next theorem, we establish a particular factorization of the Vandermonde matrix \mathbf{A}_n . This factorization serves to define a computational procedure to identify a space $\mathcal{Y}'_n \subset \mathcal{Y}_n$ satisfying (10). As a byproduct, the maximal degree N' in (19) and the rank increment sequence $(g_n)_{0 \leq n \leq \bar{N}}$ will be identified as well.

Recall that the VDM matrix \mathbf{A}_n is defined by

$$\mathbf{A}_n \triangleq \begin{bmatrix} A_0 \\ \vdots \\ A_n \end{bmatrix} \in \mathbf{R}^{(n+1)^2 \times \bar{N}}. \quad (21)$$

Theorem 9 (Structure of \mathbf{A}_n). *Let $n \geq 0$.*

The matrix \mathbf{A}_n can be factorized in the form

$$\mathbf{A}_n = \mathbf{U}_n \mathbf{E}_n \mathbf{V}_n^\top, \quad (22)$$

where

- the matrices $\mathbf{U}_n \in \mathbf{R}^{(n+1)^2 \times (n+1)^2}$, $\mathbf{V}_n \in \mathbf{R}^{\bar{N} \times \bar{N}}$ are orthogonal;
- the matrix $\mathbf{E}_n \in \mathbf{R}^{(n+1)^2 \times \bar{N}}$ is in CE form as displayed in Fig. 1 (left panel).

In particular, $\text{rank}(\mathbf{E}_n) = r_n$.

Proof. The proof is constructive. Therefore, in the course of it, recurrence formulas emerge, which play an important role in the computational procedure. It allows to identify both the degree N' and a suitable space $\mathcal{Y}'_{N'}$ in (10). We proceed by induction on the degree $n \geq 0$. First for $n = 0$, $Y_0^0(\mathbf{x}) = 1/\sqrt{4\pi}$. Therefore $\mathbf{A}_0 = \frac{1}{\sqrt{4\pi}}[1, 1, \dots, 1] \in \mathbf{R}^{1 \times \bar{N}}$. A SVD decomposition is expressed as $\mathbf{A}_0 = U_0 S_0 V_0^\top$ with

$$U_0 \triangleq [1], \quad S_0 \triangleq \left[\left(\frac{\bar{N}}{4\pi} \right)^{1/2}, 0, \dots, 0 \right], \quad V_0 \triangleq [v_1, v_2, \dots, v_{\bar{N}}], \quad (23)$$

where $V_0 \in \mathbf{R}^{\bar{N} \times \bar{N}}$ is orthogonal and $v_1 \triangleq \bar{N}^{-1/2}[1, 1, \dots, 1]^\top$. We set

$$\mathbf{U}_0 \triangleq U_0, \quad \mathbf{V}_0 \triangleq V_0, \quad \mathbf{E}_0 \triangleq S_0. \quad (24)$$

The matrix \mathbf{E}_0 has the shape displayed in Fig. 1, with $r_{-1} = 0$, $r_0 = g_0 = 1$.

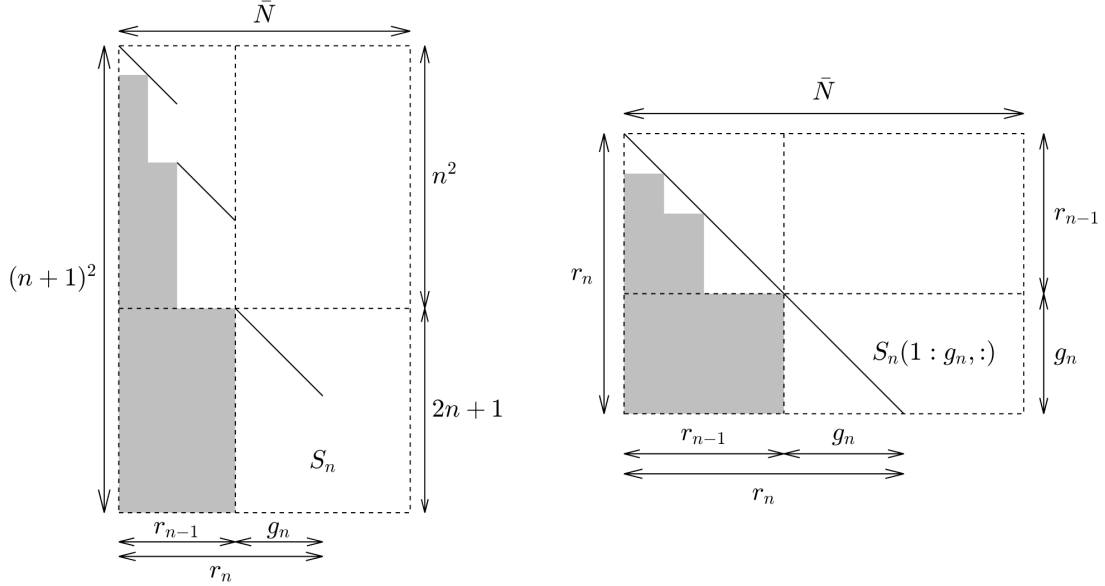


FIGURE 1. Left panel: the VDM \mathbf{A}_n is equivalent to the column echelon matrix \mathbf{E}_n , whose shape is represented on the left. Right panel: elimination of redundant lines in \mathbf{E}_n results in the lower triangular matrix \mathbf{L}_n , displayed on the right.

Assume now (induction step) that the result holds for $n-1$. We have $\mathbf{A}_{n-1} = \mathbf{U}_{n-1} \mathbf{E}_{n-1} \mathbf{V}_{n-1}^\top$ for some orthogonal matrices \mathbf{U}_{n-1} and \mathbf{V}_{n-1} , and for \mathbf{E}_{n-1} in CE form as in Fig. 1. Consider the matrix

$$\begin{aligned} \begin{bmatrix} \mathbf{U}_{n-1}^\top & \mathbf{0}_{n^2, 2n+1} \\ \mathbf{0}_{2n+1, n^2} & \mathbf{I}_{2n+1} \end{bmatrix} \mathbf{A}_n \mathbf{V}_{n-1} &= \begin{bmatrix} \mathbf{U}_{n-1}^\top & \mathbf{0}_{n^2, 2n+1} \\ \mathbf{0}_{2n+1, n^2} & \mathbf{I}_{2n+1} \end{bmatrix} \begin{bmatrix} \mathbf{A}_{n-1} \\ \mathbf{A}_n \end{bmatrix} \mathbf{V}_{n-1} \\ &= \begin{bmatrix} \mathbf{U}_{n-1}^\top & \mathbf{0}_{n^2, 2n+1} \\ \mathbf{0}_{2n+1, n^2} & \mathbf{I}_{2n+1} \end{bmatrix} \begin{bmatrix} \mathbf{U}_{n-1} \mathbf{E}_{n-1} \mathbf{V}_{n-1}^\top \\ \mathbf{A}_n \end{bmatrix} \mathbf{V}_{n-1} \\ &= \begin{bmatrix} \mathbf{E}_{n-1} \\ \mathbf{A}_n \mathbf{V}_{n-1} \end{bmatrix}. \end{aligned} \quad (25)$$

Using the CE form of \mathbf{E}_{n-1} shown in Fig. 1, we have

$$\begin{bmatrix} \mathbf{E}_{n-1} \\ \mathbf{A}_n \mathbf{V}_{n-1} \end{bmatrix} = \begin{bmatrix} \mathbf{E}_{n-1}(\llbracket 1 : n^2 \rrbracket, \llbracket 1 : r_{n-1} \rrbracket) & \mathbf{0}_{n^2, \bar{N}-r_{n-1}} \\ \mathbf{A}_n \mathbf{V}_{n-1}(\llbracket 1 : \bar{N} \rrbracket, \llbracket 1 : r_{n-1} \rrbracket) & \mathbf{A}_n \mathbf{V}_{n-1}(\llbracket 1 : \bar{N} \rrbracket, \llbracket r_{n-1} + 1 : \bar{N} \rrbracket) \end{bmatrix}. \quad (26)$$

The orthogonal matrices \mathbf{U}_n , \mathbf{V}_n and the block diagonal matrix \mathbf{S}_n are defined by the SVD of the block in position (2, 2) in (26)

$$\mathbf{A}_n \mathbf{V}_{n-1}(\llbracket 1 : \bar{N} \rrbracket, \llbracket r_{n-1} + 1 : \bar{N} \rrbracket) \triangleq \mathbf{U}_n \mathbf{S}_n \mathbf{V}_n^\top. \quad (27)$$

By definition of the SVD, \mathbf{U}_n and \mathbf{V}_n are orthogonal, whereas \mathbf{S}_n is diagonal, with nonnegative and nonincreasing values along the diagonal. This gives that (25) can be expressed as

$$\begin{bmatrix} \mathbf{U}_{n-1}^\top & \mathbf{0}_{n^2, 2n+1} \\ \mathbf{0}_{2n+1, n^2} & \mathbf{I}_{2n+1} \end{bmatrix} \mathbf{A}_n \mathbf{V}_{n-1} = \begin{bmatrix} \mathbf{E}_{n-1}(\llbracket 1 : n^2 \rrbracket, \llbracket 1 : r_{n-1} \rrbracket) & \mathbf{0}_{n^2, \bar{N}-r_{n-1}} \\ \mathbf{A}_n \mathbf{V}_{n-1}(\llbracket 1 : \bar{N} \rrbracket, \llbracket 1 : r_{n-1} \rrbracket) & \mathbf{U}_n \mathbf{S}_n \mathbf{V}_n^\top \end{bmatrix}. \quad (28)$$

Multiplying (28) on the left by $\begin{bmatrix} \mathbf{I}_{n^2} & \mathbf{0}_{n^2, 2n+1} \\ \mathbf{0}_{2n+1, n^2} & \mathbf{U}_n^\top \end{bmatrix}$, and on the right by $\begin{bmatrix} \mathbf{I}_{n^2} & \mathbf{0}_{n^2, 2n+1} \\ \mathbf{0}_{2n+1, n^2} & \mathbf{V}_n \end{bmatrix}$, yields $\mathbf{U}_n^\top \mathbf{A}_n \mathbf{V}_n = \mathbf{E}_n$, where the matrices \mathbf{U}_n , \mathbf{V}_n , \mathbf{E}_n are defined by

$$\begin{cases} \mathbf{U}_n \triangleq \begin{bmatrix} \mathbf{U}_{n-1} & \mathbf{0}_{n^2, 2n+1} \\ \mathbf{0}_{2n+1, n^2} & \mathbf{U}_n \end{bmatrix}, & \mathbf{V}_n \triangleq \mathbf{V}_{n-1} \begin{bmatrix} \mathbf{I}_{n^2} & \mathbf{0} \\ \mathbf{0} & \mathbf{V}_n \end{bmatrix}, \\ \mathbf{E}_n \triangleq \begin{bmatrix} \mathbf{E}_{n-1}(\llbracket 1 : n^2 \rrbracket, \llbracket 1 : r_{n-1} \rrbracket) & \mathbf{0}_{n^2, \bar{N}-r_{n-1}} \\ \mathbf{U}_n^\top \mathbf{A}_n \mathbf{V}_{n-1}(\llbracket 1 : n^2 \rrbracket, \llbracket 1 : r_{n-1} \rrbracket) & \mathbf{S}_n \end{bmatrix}. \end{cases} \quad (29)$$

The matrices \mathbf{U}_n and \mathbf{V}_n are orthogonal and satisfy (22). Furthermore it turns out that the matrix \mathbf{E}_n defined in (29) is in CE form. Concerning the ranks, combining (22) and (29) proves that $r_n = \text{rank } \mathbf{E}_n = r_{n-1} + \text{rank } \mathbf{S}_n$. At the end,

$$\text{rank } \mathbf{S}_n = g_n, \quad (30)$$

and \mathbf{E}_n has exactly the shape shown in Fig. 1. This completes the proof. \square

As already mentioned, the steps in the proof of Theorem 9 can be turned into a computational algorithm, with a loop over the integer n , as follows.

Algorithm 10. For $n \geq 0$,

1. compute the matrix A_n ;
2. compute the matrices U_n, S_n, V_n , by SVD of the matrix in (27), ((23) for $n = 0$);
3. assemble the matrices E_n, V_n and U_n by (29), ((24) for $n = 0$);
4. compute the rank increment g_n by (30), and the rank $r_n = r_{n-1} + g_n$.

Stopping criterion: the algorithm exits exactly when $r_n = \bar{N} = 6N^2 + 2$.

Corollary 11. (i) For every $n \geq 0$, the columns of $V_n(\llbracket 1 : \bar{N} \rrbracket, \llbracket r_n + 1 : \bar{N} \rrbracket)$ are an orthonormal basis of $\text{Ker } A_n$.

(ii) For every $n \geq 1$, the columns of $U_n(\llbracket 1 : \bar{N} \rrbracket, \llbracket 1 : g_n \rrbracket)$ are an orthonormal basis of $\text{Ran}(A_n V_{n-1}(\llbracket 1 : \bar{N} \rrbracket, \llbracket r_{n-1} + 1 : \bar{N} \rrbracket))$.

We consider now the functional interpretation of Algorithm 10. It allows to define a particular Spherical Harmonics subspace, which provides a solution to the problem (CS/HS). First we define the functions $u_n^i(\mathbf{x})$ as follows.

Definition 12 (Functions u_n^i). For all $0 \leq n \leq N'$ and $1 \leq i \leq 2n + 1$, the Spherical Harmonics $u_n^i(\mathbf{x}) \in Y_n$ is defined from the i -th column vector of the matrix U_n by

$$u_n^i(\mathbf{x}) := [Y_n^m(\mathbf{x})]_{-n \leq m \leq n}^\top U_n(\llbracket 1 : \bar{N} \rrbracket, i). \quad (31)$$

The u_n^i form an orthonormal family of Y_n .

Definition 13 (SH spaces Y'_n and \mathcal{Y}'_n). (i) For all $0 \leq n \leq N'$, we call Y'_n and Y''_n the spaces defined by

$$Y'_n \triangleq \text{Span}\{u_n^i, 1 \leq i \leq g_n\} \subset Y_n, \quad Y''_n \triangleq \text{Span}\{u_n^i, g_n + 1 \leq i \leq 2n + 1\} \quad (32)$$

and

$$Y_n = Y'_n \oplus Y''_n. \quad (33)$$

(ii) The SH subspace $\mathcal{Y}'_{N'}$ is defined by

$$\mathcal{Y}'_{N'} \triangleq Y'_0 \oplus \cdots \oplus Y'_{N'} = \text{Span}\{u_n^i, 1 \leq i \leq g_n, 0 \leq n \leq N'\}. \quad (34)$$

Note that the spaces Y''_n , Y'_n , and $\mathcal{Y}'_{N'}$ are intrinsically defined; they can be defined independently of our algorithm. Indeed, the space Y''_n represents the space of SH functions of degree n which are “incorrectly represented” on the Cubed Sphere CS_N . This means that their restriction to CS_N coincide with the restriction of a SH functions of smaller degree. This is expressed as follows.

Corollary 14 (Interpretation of the space Y''_n). For $n \geq 1$, the SH subspace Y''_n satisfies

$$Y''_n = \{f \in Y_n : f|_{\text{CS}_N} \in \text{Ran } A_{n-1}^\top\} = \{f \in Y_n : \exists g \in Y_0 \oplus \cdots \oplus Y_{n-1}, f|_{\text{CS}_N} = g|_{\text{CS}_N}\}.$$

Proof. Let $\Pi_{\text{Ker } A_{n-1}}$, (resp. $\Pi_{\text{Ran } A_{n-1}^\top}$) be the matrix of the orthogonal projection on $\text{Ker } A_{n-1}$, (resp. on $\text{Ran } A_{n-1}^\top$). Then the columns of the matrix $V_{n-1}(\llbracket 1 : \bar{N} \rrbracket, \llbracket r_{n-1} + 1 : \bar{N} \rrbracket)$ form an orthonormal basis of $\text{Ker } A_{n-1}$. Similarly, the columns of the matrix $U_n(\llbracket 1 : \bar{N} \rrbracket, \llbracket 1 : g_n \rrbracket)$ form an orthonormal basis of the space $\text{Ran } A_n V_{n-1}(\llbracket 1 : \bar{N} \rrbracket, \llbracket r_{n-1} + 1 : \bar{N} \rrbracket)$. Therefore, the columns of $U_n(\llbracket 1 : \bar{N} \rrbracket, \llbracket 1 : g_n \rrbracket)$ form an orthonormal basis of the space $\text{Ran}(A_n \Pi_{\text{Ker } A_{n-1}}) = \left(\text{Ker}(\text{I} - \Pi_{\text{Ran } A_{n-1}^\top}) A_n^\top \right)^\perp$. This space represents the Spherical Harmonics of degree n with restriction to CS_N in $\text{Ran } A_{n-1}^\top$. This means that when restricted to CS_N , they coincide with Spherical Harmonics of lower degree. \square

Remark 15. In [7, p. 602], a method is considered to numerically identify the subspace $\text{Ker } M_1 \cap \text{Ker } M_2$, where M_1 and M_2 are two matrices. The following SVDs are evaluated

$$\begin{cases} M_1 = U_1 S_1 V_1^\top, \\ M_2 V_1 = U_2 S_2 V_2^\top \end{cases} \quad (35)$$

The space $\text{Ker } M_1 \cap \text{Ker } M_2$ is deduced from the knowledge of the matrices S_1, V_1 and S_2, V_2 . The factorization in (25) in our approach uses a similar idea. However, a first difference is that our method uses (35) iteratively and not just once. Second, our goal is to identify a range subspace and not a kernel. Indeed, at step n , the orthonormal basis $U_n(\llbracket 1 : \bar{N} \rrbracket, \llbracket 1 : g_n \rrbracket)$ of the space $\text{Ran } A_n V_{n-1}(\llbracket 1 : \bar{N} \rrbracket, \llbracket r_{n-1} + 1 : \bar{N} \rrbracket)$ is stored, since it defines the orthonormal basis $(u_n^i)_{1 \leq i \leq g_n}$ of $Y'_n \subset \mathcal{Y}'_{N'}$.

4.3. Row compression. Consider again the factorization (22). It is expressed as

$$\mathbf{U}_n^\top \mathbf{A}_n = \mathbf{E}_n \mathbf{V}_n^\top. \quad (36)$$

We perform a row compression by eliminating redundant rows in (36). This leads to define the matrices $\tilde{\mathbf{U}}_n \in \mathbf{R}^{(n+1)^2 \times r_n}$ and $\mathbf{L}_n \in \mathbf{R}^{r_n \times \bar{N}}$ by

$$\tilde{\mathbf{U}}_n \triangleq \begin{bmatrix} U_0(\llbracket 1 : 1 \rrbracket, \llbracket 1 : g_0 \rrbracket) & & \\ & \ddots & \\ & & U_n(\llbracket 1 : 2n+1 \rrbracket, \llbracket 1 : g_n \rrbracket) \end{bmatrix}, \quad (37)$$

$$\mathbf{L}_n \triangleq \begin{bmatrix} \mathbf{I}_1(\llbracket 1 : g_0 \rrbracket, \llbracket 1 : 1 \rrbracket) & & \\ & \ddots & \\ & & \mathbf{I}_{2n+1}(\llbracket 1 : g_n \rrbracket, \llbracket 1 : 2n+1 \rrbracket) \end{bmatrix} \mathbf{E}_n. \quad (38)$$

The matrix \mathbf{L}_n in (38) is lower triangular. It contains the pivot rows of the column echelon matrix \mathbf{E}_n . Doing so, the rows of S_k , $k \leq n$, with nonzero singular values are conserved and the zero rows of S_k are eliminated. This is summarized in the following corollary.

Corollary 16. (i) The matrix $\tilde{\mathbf{U}}_n^\top \mathbf{A}_n$ admits the LQ factorization

$$\tilde{\mathbf{U}}_n^\top \mathbf{A}_n = \mathbf{L}_n \mathbf{V}_n^\top, \quad (39)$$

where the matrix \mathbf{L}_n is lower triangular and has full row rank r_n , and $\tilde{\mathbf{U}}_n$ satisfies the orthogonality relation $\tilde{\mathbf{U}}_n^\top \tilde{\mathbf{U}}_n = \mathbf{I}_{r_n}$.

(ii) In particular, for the degree $n = N'$ in (19), we have $r_{N'} = \bar{N}$ and the matrix $\mathbf{A}_{N'}$ has full column rank. The factorization (39) of $\mathbf{A}_{N'}$

$$\tilde{\mathbf{U}}_{N'}^\top \mathbf{A}_{N'} = \mathbf{L}_{N'} \mathbf{V}_{N'}^\top, \quad (40)$$

is such that the lower triangular matrix $\mathbf{L}_{N'} \in \mathbf{R}^{\bar{N} \times \bar{N}}$ is non singular.

The compressed factorization (40) now gives a solution to the interpolation problem (CS/HS).

Corollary 17 (Solution to Problem (CS/HS)). The space $\mathcal{Y}'_{N'}$ is unisolvent for the Lagrange interpolation problem (CS/HS), i.e.

$$\forall \mathbf{y} \in \mathbf{R}^{\bar{N}}, \exists! u \in \mathcal{Y}'_{N'}, \quad u(\mathbf{x}_j) = y_j, \quad 1 \leq j \leq \bar{N}. \quad (41)$$

The SH function $u(\mathbf{x})$ is expressed in the basis Y_n^m by

$$\begin{cases} u(\mathbf{x}) = [\mathbf{Y}_n^m(\mathbf{x})]_{|m| \leq n \leq N'}^\top \tilde{\mathbf{U}}_{N'} \boldsymbol{\alpha}, \\ \boldsymbol{\alpha} = (\mathbf{L}_{N'}^\top)^{-1} \mathbf{V}_{N'}^\top \mathbf{y}. \end{cases} \quad (42)$$

The vector $\boldsymbol{\alpha}$ is obtained by backward substitution in the upper triangular system $\mathbf{L}_{N'}^\top \boldsymbol{\alpha} = \mathbf{V}_{N'}^\top \mathbf{y}$.

Proof. Let $u \in \mathcal{Y}'_{N'}$. There exists a unique family of \bar{N} reals,

$$\boldsymbol{\alpha} = (\alpha_n^i)_{0 \leq n \leq N', 1 \leq i \leq g_n},$$

such that

$$u(\cdot) = \sum_{0 \leq n \leq N'} \sum_{1 \leq i \leq g_n} \alpha_n^i u_n^i(\cdot) = [\mathbf{Y}_n^m(\cdot)]_{|m| \leq n \leq N'}^\top \tilde{\mathbf{U}}_{N'} \boldsymbol{\alpha}. \quad (43)$$

By Theorem 16, we have

$$[u(\mathbf{x}_j)]_{1 \leq j \leq \bar{N}} = \mathbf{A}_{N'}^\top \tilde{\mathbf{U}}_{N'} \boldsymbol{\alpha} = \mathbf{V}_{N'} \mathbf{L}_{N'}^\top \boldsymbol{\alpha}, \quad (44)$$

where $\mathbf{V}_{N'}$ is orthogonal, and $\mathbf{L}_{N'}$ is lower triangular and nonsingular. Therefore the SH function $u(\mathbf{x})$ interpolates the data $\mathbf{y} \in \mathbf{R}^{\bar{N}}$ on CS_N if, and only if, the vector $\boldsymbol{\alpha}$ satisfies $\mathbf{V}_{N'} \mathbf{L}_{N'}^\top \boldsymbol{\alpha} = \mathbf{y}$, which is equivalent to $\boldsymbol{\alpha} = (\mathbf{L}_{N'}^\top)^{-1} \mathbf{V}_{N'}^\top \mathbf{y}$. \square

¹LQ factorization is identical to QR factorization up to transposition.

5. NUMERICAL RESULTS

5.1. Numerical estimate of the rank increment. Let $N \geq 0$ be the integer representing the accuracy of the Cubed Sphere CS_N . Corollary 5 asserts that Algorithm 10 necessarily exits after a finite number of iterations on n with exit index $n = N'$, defined in (19). Regarding the rank increment g_n , Theorem 9 shows that $g_n = \text{rank } S_n$ is the number of nonzero singular values of S_n , see (30). Thus g_n is numerically estimated by some thresholding of the diagonal of S_n . This kind of thresholding is commonly used to numerically determine the rank of a given matrix by using the SVD². Here, we have used such a rank evaluation to infer the value $\text{rank}(\mathbf{A}_n) - \text{rank}(\mathbf{A}_{n-1})$. This value has been systematically tabulated with Matlab. Table 1 reports the rank increment in \mathbf{A}_n for N increasing from $N = 1$ (Cubed Sphere with 8 nodes) to $N = 6$ (Cubed Sphere with 218 nodes). This has led to the following claim.

Claim 18. (1) \mathbf{A}_{2N-1} has full row rank. Equivalently, $r_{2N-1} = 4N^2$.

(2) \mathbf{A}_{3N} has full column rank. Equivalently, $r_{3N} = \bar{N}$.

(3) The sequence of rank increments g_n in (18) is numerically observed as given by

$$g_0 = 1, \quad g_n = \begin{cases} 2n + 1, & 1 \leq n \leq 2N - 1, \\ 4(3N - n) - 2, & 2N \leq n \leq 3N - 2, \\ 3, & n = 3N - 1, \\ 1, & n = 3N. \end{cases}$$

From now on, if not otherwise mentioned, Claim 18 will be used to further perform numerical approximations. In particular we assume that $r_{2N-1} = 4N^2$ for $n = 2N - 1$, and $r_{3N} = \bar{N} = 6N^2 + 2$ for $n = 3N$.

	0	1	2	3	4	5	6	7	8	9	10	11	12	13	14	15	16	17	18
1	1	3	3	1															
2	1	3	5	7	6	3	1												
3	1	3	5	7	9	11	10	6	3	1									
4	1	3	5	7	9	11	13	15	14	10	6	3	1						
5	1	3	5	7	9	11	13	15	17	19	18	14	10	6	3	1			
6	1	3	5	7	9	11	13	15	17	19	21	23	22	18	14	10	6	3	1

TABLE 1. Numerically evaluated rank increment g_n of the Vandermonde matrix \mathbf{A}_n , for $1 \leq N \leq 6$ (row), $0 \leq n \leq 3N$ (column). The matlab function `rank` has been used.

Some consequences of Claim 18 are as follows.

(1) The smallest $n \geq 0$ such that $r_n = \bar{N}$ is

$$N' = 3N. \quad (45)$$

(2) For every $0 \leq n \leq 2N - 1$, $Y'_n = Y_n$. In particular, the unisolvent space \mathcal{Y}'_{3N} contains all SH of degree $n < 2N$, i.e. $Y_0 \oplus \cdots \oplus Y_{2N-1} \subset \mathcal{Y}'_{3N}$. We call

$$\mathcal{Y}'_a = Y_0 \oplus \cdots \oplus Y_{2N-1}. \quad (46)$$

(3) For all $2N \leq n \leq 3N$, $Y'_n \subsetneq Y_n$. There exists a SH of degree n , $f \in Y_n$, such that $f \notin \mathcal{Y}'_{3N}$. We call

$$\mathcal{Y}'_b = Y'_{2N} \oplus \cdots \oplus Y'_{3N}. \quad (47)$$

In summary, assuming that Claim 18 holds, the SH subspace attached to the Cubed Sphere CS_N by the analysis above is the space \mathcal{Y}'_{3N} . It is decomposed as

$$\mathcal{Y}'_{3N} = \mathcal{Y}'_a \oplus \mathcal{Y}'_b. \quad (48)$$

As a corollary, we have that for all $n > 3N$ and $f \in Y_n$, there exists $u \in \mathcal{Y}'_{3N}$ such that $f|_{\text{CS}_N} = u|_{\text{CS}_N}$.

Remark 19. A proof of Claim 18 is open for the moment.

Remark 20. In (20), an upper bound of N' has been proved to be

$$N' \leq \lceil \frac{7.5\pi}{(1-\epsilon)\text{sep}(\text{CS}_N)} \rceil, \quad (49)$$

where $0 < \epsilon < 1$ is arbitrary small. One may wonder how (49) compares to the value $N' = 3N$ in (45). The analysis in [2] has established that the shortest geodesic distance $\text{sep}(\text{CS}_N)$ is realized for any short arc

²This is the principle behind the `rank` function in Matlab.

around the center of any edge on the Cubed Sphere. Expressing this distance in terms of the Cubed Sphere step angle $\pi/2N$ (equatorial grid size), it turns out that

$$\text{sep}(\text{CS}_N) \sim \frac{\sqrt{2}}{2} \frac{\pi}{2N}.$$

A straightforward consequence is that the upper bound above behaves like

$$\frac{5\sqrt{2}}{1-\epsilon} N' \approx 7.07 N', \quad (50)$$

which is a significantly larger value than N' .

5.2. Truncation analysis. Approximating functions on the sphere is commonly obtained with a truncated Spherical Harmonic series. A function $\mathbf{x} \in \mathbb{S}^2 \mapsto f(\mathbf{x})$ is expanded as

$$f(\lambda, \theta) = \sum_{n=0}^{+\infty} \sum_{|m| \leq n} f_n^m Y_n^m(\lambda, \theta), \quad (51)$$

or equivalently

$$f(\lambda, \theta) = \sum_{|m|=0}^{+\infty} \sum_{n=|m|}^{+\infty} f_n^m Y_n^m(\lambda, \theta). \quad (52)$$

A first truncation pattern is the *triangular* scheme. It consists in defining $f_T \simeq f$ by the finite sum

$$f_T(\lambda, \theta) = \sum_{n=0}^{N_T} \sum_{|m| \leq \min(n, M_T)} f_n^m Y_n^m(\lambda, \theta). \quad (53)$$

Here M_T, N_T are parameters defining the truncation.

A second truncation is the *rhomboidal* scheme. We define $f_R \simeq f$ by

$$f_R(\lambda, \theta) = \sum_{|m| \leq M_R} \sum_{n=m}^{m+N_R} f_n^m Y_n^m(\lambda, \theta). \quad (54)$$

Both truncations are represented in Fig 2. In [6] the two truncations are compared in the context of ocean

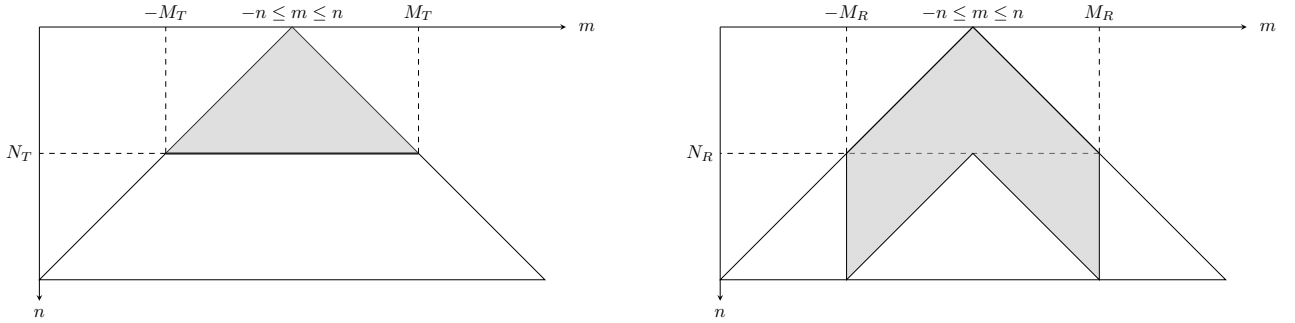


FIGURE 2. Left: triangular truncation with parameters M_T and N_T . Right: rhomboidal truncation with parameters M_R and N_R .

numerical simulations in the case $M_T = N_T$ and $M_R = N_R$.

Here we are interested in identifying which truncation is related to the approximation with the space \mathcal{Y}'_{3N} in (48). In our case, there is no additional parameter to select to define a particular truncation. The truncation, which necessarily occurs, automatically emerges from the relations (45)-(46).

The approximation space \mathcal{Y}'_{3N} in (48) is decomposed as

$$\mathcal{Y}'_{3N} = \mathcal{Y}'_a \oplus \mathcal{Y}'_b. \quad (55)$$

Consider a given function $Y_n^m(\mathbf{x})$, $n \geq 0$, $|m| \leq n$. The truncation scheme of the space \mathcal{Y}'_{3N} is evaluated by using the least square value

$$d(Y_n^m, \mathcal{Y}'_{3N}) \triangleq \|Y_n^m - \Pi_{\mathcal{Y}'_{3N}} Y_n^m\|_2, \quad (56)$$

where $\Pi_{\mathcal{Y}'_{3N}} Y_n^m \in \mathcal{Y}'_{3N}$ stands for the orthogonal projection of Y_n^m on \mathcal{Y}'_{3N} . They are three cases.

- (1) $n < 2N$. In this case, $d(Y_n^m, \mathcal{Y}'_{3N}) = 0$. This means that $Y_n^m \in \mathcal{Y}'_a \subset \mathcal{Y}'_{3N}$.
- (2) $n > 3N$. In this case, $d(Y_n^m, \mathcal{Y}'_{3N}) = 1$. This means that Y_n^m is orthogonal to \mathcal{Y}'_{3N} .

(3) $2N \leq n \leq 3N$. This is the region where the truncation occurs. This case is analyzed below.

The orthogonal projector on \mathcal{Y}'_{3N} , (resp. on $(\mathcal{Y}'_{3N})^\perp$), is represented by the matrix $\tilde{U}_{3N}\tilde{U}_{3N}^\top$, (resp. $I - \tilde{U}_{3N}\tilde{U}_{3N}^\top$). We have

$$[d(Y_n^m, \mathcal{Y}'_{3N})]_{|m| \leq n \leq 3N} = \left[\|c_j(I - \tilde{U}_{3N}\tilde{U}_{3N}^\top)\|_2 \right]_{1 \leq j \leq \bar{N}}, \quad (57)$$

where $c_j(M)$ stands for the column j of the matrix M . In Table 2, the distance $d(Y_n^m, \mathcal{Y}'_{3N})$ is reported in the case of the Cubed Sphere CS_2 ($N = 2$). The results are in conformity with the case 1. above, where $\mathcal{Y}'_1 = \bigoplus_{n \leq 2N-1} Y_n \subset \mathcal{Y}'_{3N}$. The distances of Table 2 are reported in logarithmic scale in Fig. 3 (top-left panel). The same results for $N = 4, 8, 16, 32$ are reported in the same fashion in the left side in Fig. 3. As can be observed, some *rhomboidal* pattern emerges for the case 3. (case $2N \leq n \leq 3N$). Two regimes of (n, m) appear:

- Y_n^m is accurately approximated by the space \mathcal{Y}'_{3N} if $M_n \leq |m| < 2N$, where $n \mapsto M_n$ is some increasing function;
- Y_n^m is orthogonal to the approximation space \mathcal{Y}'_{3N} for $|m| > 2N$, and for $|m| < M_n$.

	-6	-5	-4	-3	-2	-1	0	1	2	3	4	5	6
0							0						
1						0	4.7e-17	4.7e-17					
2					0	6.2e-16	7.6e-17	2.3e-16	3.5e-16				
3				2.2e-16	7.7e-17	2.2e-16	3.3e-16	3.6e-16	4.9e-16	3.2e-16			
4			1	0.35	5.1e-16	0.94	4.8e-16	0.94	1.6e-15	0.35	9.3e-16		
5		0.99	1	0.32	1	0.96	0.89	0.96	1	0.32	0.45	0.99	
6	1	1	1	1	1	1	0.94	1	1	1	0.35	1	1

TABLE 2. Distance $d(Y_n^m, \mathcal{Y}'_{3N}) = \|Y_n^m - \Pi_{\mathcal{Y}'_{3N}} Y_n^m\|_2$, for $0 \leq n \leq 3N$ (rows), $-n \leq m \leq n$ (columns); $N = 2$.

5.3. SVD factorization of the VDM matrix $\mathbf{A}_{N'}$. In Section 4.1, a particular echelon form has been used as a building block to obtain a factorization of Vandermonde matrices. One may wonder how this compares to the more standard SVD factorization. Here we consider the alternative of using the SVD decomposition of the full VDM matrix $\mathbf{A}_{N'}$, instead of (40). It is given by

$$\mathbf{U}_{\text{SVD}}^\top \mathbf{A}_{N'} = \mathbf{S}_{\text{SVD}} \mathbf{V}_{\text{SVD}}^\top.$$

This factor form gives that the matrix $\mathbf{U}_{\text{SVD}} \in \mathbf{R}^{(N'+1)^2 \times \bar{N}}$ contains an orthonormal basis of $\text{Ran } \mathbf{A}_{N'}$. The matrix $\mathbf{V}_{\text{SVD}} \in \mathbf{R}^{\bar{N} \times \bar{N}}$ is orthogonal, and $\mathbf{S}_{\text{SVD}} \in \mathbf{R}^{\bar{N} \times \bar{N}}$ is diagonal, nonsingular and has the positive singular values of $\mathbf{A}_{N'}$ on the diagonal. Suppose that, according to Claim 18, it holds that $N' = 3N$. Then, an approximation space $\mathcal{Y}'_{\text{SVD}}$ is deduced from the columns of \mathbf{U}_{SVD} . This space is a priori different from the space \mathcal{Y}'_{3N} in (48). The interpolating function associated to the set of data $\mathbf{y} \in \mathbf{R}^{\bar{N}}$ is given by

$$u_{\text{SVD}}(\mathbf{x}) = [Y_n^m(\mathbf{x})]_{|m| \leq n \leq 3N}^\top (\mathbf{A}_{3N}^\top)^\dagger \mathbf{y}, \quad \text{with} \quad (\mathbf{A}_{3N}^\top)^\dagger \triangleq \mathbf{U}_{\text{SVD}} \mathbf{S}_{\text{SVD}}^{-1} \mathbf{V}_{\text{SVD}}^\top.$$

Here, $(\mathbf{A}_{3N}^\top)^\dagger$ is the Moore-Penrose inverse of \mathbf{A}_{3N}^\top .

We now comment on how the two spaces \mathcal{Y}'_{3N} and $\mathcal{Y}'_{\text{SVD}}$ compare in terms of approximation power. Table 3, is the counterpart of Table 2 when replacing the space \mathcal{Y}'_{3N} by the space $\mathcal{Y}'_{\text{SVD}}$. Similarly, in Fig. 3, the right column is the counterpart of the left column. As can be observed, the truncation pattern is different for \mathcal{Y}'_{3N} and $\mathcal{Y}'_{\text{SVD}}$: when using $\mathcal{Y}'_{\text{SVD}}$ the nonzero distances are smaller. But the proportion of the well represented SH is also smaller. Notice nonzero distances in the region $N \leq n \leq 2N$. Overall, the space $\mathcal{Y}'_{\text{SVD}}$ has less approximation power than \mathcal{Y}'_{3N} .

Table 4 reports a repartition analysis of the distance values when using each subspace, $\mathcal{Y}'_{\text{SVD}}$ and \mathcal{Y}'_{3N} . At least 25% of the $Y_n^m, n \leq 3N$, are in the space \mathcal{Y}'_{3N} . And at least 25% are almost orthogonal to \mathcal{Y}'_{3N} . The interquartile $Q_3 - Q_1$ and the standard deviation indicate that the distances are less dispersed in the SVD approach. The first quartile in the SVD case is larger than the median in the echelon case. In particular a larger proportion of the $Y_n^m, n \leq 3N$, is accurately interpolated in \mathcal{Y}'_{3N} than in $\mathcal{Y}'_{\text{SVD}}$. Finally, the observed minimum value $3.8 \cdot 10^{-4}$ for the SVD approach with $N = 4$ indicates that none of the Y_n^m belongs to the space $\mathcal{Y}'_{\text{SVD}}$. Moreover, the median $1.4 \cdot 10^{-3}$ ($N = 32$) shows that half of the $Y_n^m, n \leq 3N$, are well represented in \mathcal{Y}'_{3N} . Finally we plot the histograms of the distances for $N = 32$ in Fig. 4. Again, these histograms support the preference to the subspace \mathcal{Y}'_{3N} compared to $\mathcal{Y}'_{\text{SVD}}$. The picture is as follows. Either

	-6	-5	-4	-3	-2	-1	0	1	2	3	4	5	6
0							8.3e-16						
1						9.9e-16	8.3e-16	1.2e-15					
2					0.68	0.68	0.74	0.68	0.74				
3				0.71	1.1e-15	0.68	0.75	0.68	0.64	0.71			
4			1	0.75	0.71	0.97	0.15	0.97	0.23	0.75	0.18		
5		0.71	1	0.25	1	0.69	0.59	0.69	0.77	0.25	0.3	0.71	
6	0.71	0.84	1	0.84	0.73	0.79	0.59	0.79	0.9	0.84	0.22	0.84	0.76

TABLE 3. Distance $d(Y_n^m, \mathcal{Y}'_{\text{SVD}}) = \|Y_n^m - \Pi_{\mathcal{Y}'_{\text{SVD}}} Y_n^m\|_2$, for $0 \leq n \leq 3N$ (rows), $-n \leq m \leq n$ (columns); $N = 2$.

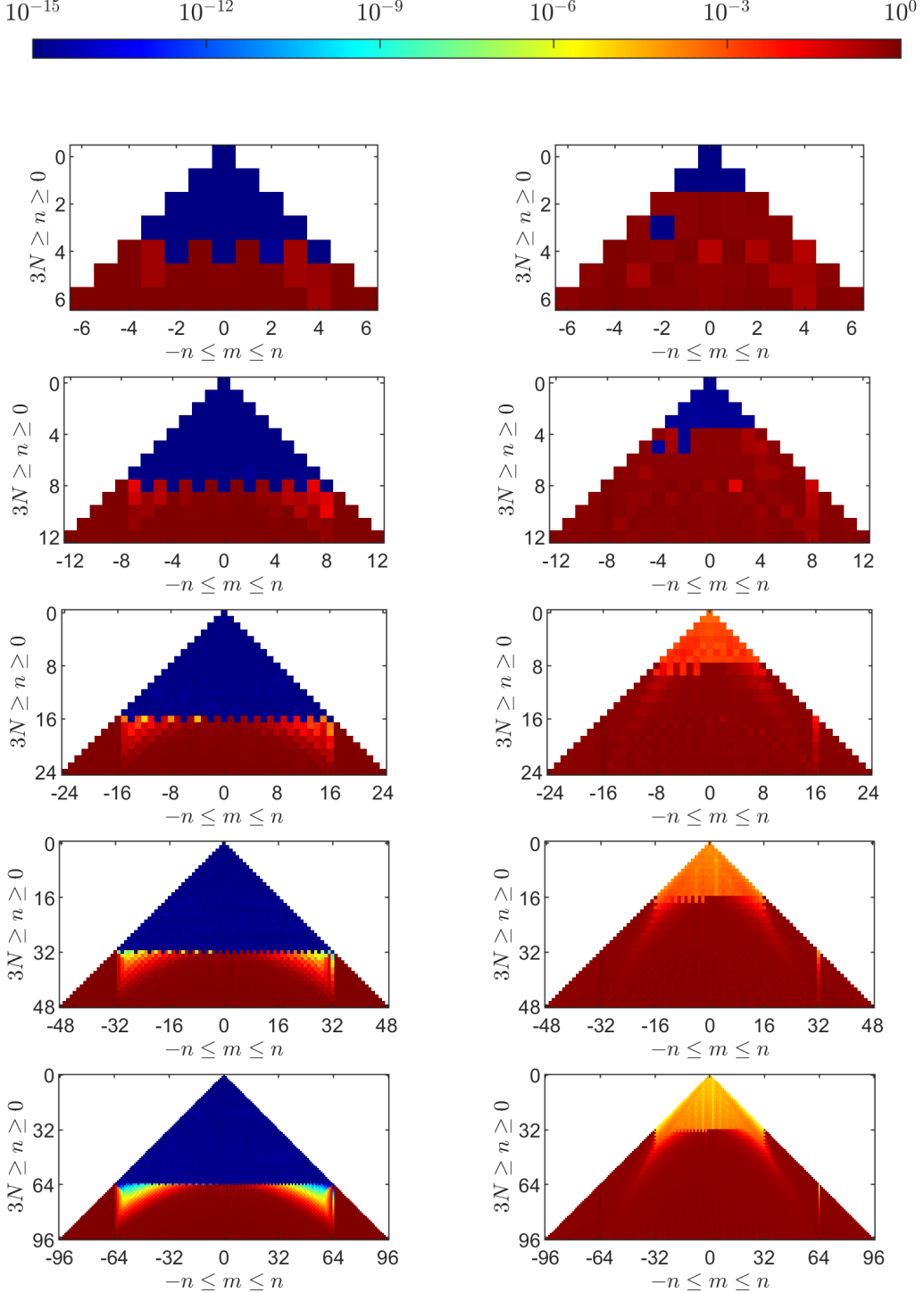


FIGURE 3. Left column: distance $d(Y_n^m, \mathcal{Y}'_{3N})$. Right column: distance $d(Y_n^m, \mathcal{Y}'_{\text{SVD}})$. From top to bottom line: $N = 2, 4, 8, 16$ and 32 .

	$d(Y_n^m, \mathcal{Y}'_{3N})$							$d(Y_n^m, \mathcal{Y}'_{\text{SVD}})$						
N	min	Q1	median	Q3	max	mean	std	min	Q1	median	Q3	max	mean	std
2	0	3.5e-16	0.35	1	1	0.51	0.47	8.3e-16	0.52	0.71	0.79	1	0.62	0.3
4	0	5.9e-16	0.37	0.99	1	0.46	0.46	1.7e-15	0.52	0.69	0.73	1	0.59	0.27
8	0	8.8e-16	0.1	0.98	1	0.42	0.45	0.00038	0.48	0.68	0.71	1	0.56	0.26
16	0	1.1e-15	0.024	0.93	1	0.4	0.45	3.1e-05	0.48	0.67	0.71	1	0.54	0.26
32	0	1.4e-15	0.0014	0.91	1	0.39	0.44	2.3e-08	0.45	0.66	0.71	1	0.53	0.26

TABLE 4. Comparison statistics of the distances $d(Y_n^m, \mathcal{Y}'_{3N})$ and $d(Y_n^m, \mathcal{Y}'_{\text{SVD}})$, for $|m| \leq n \leq 3N$: minimum, first quartile, median, third quartile, maximum, mean and standard deviation.

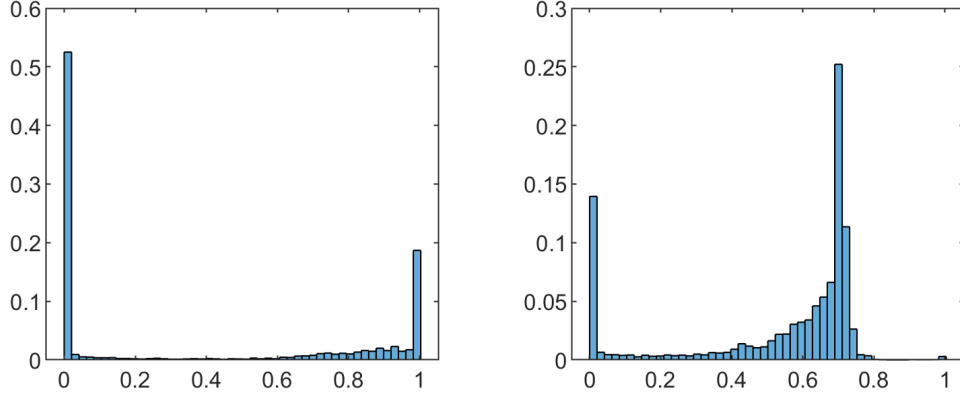


FIGURE 4. Histogram of the distances $d(Y_n^m, \mathcal{Y}'_{3N})$ (left panel) and $d(Y_n^m, \mathcal{Y}'_{\text{SVD}})$ (right panel), with $|m| \leq n \leq 3N = 3 \cdot 32$.

Y_n^m almost belongs to \mathcal{Y}'_{3N} , either Y_n^m is almost orthogonal to \mathcal{Y}'_{3N} . And more that 50% of the Y_n^m almost belong to \mathcal{Y}'_{3N} , whereas less than 15% are close to $\mathcal{Y}'_{\text{SVD}}$.

In conclusion, the incremental approach in Algorithm 10 has led to associate the approximation space \mathcal{Y}'_{3N} to the grid CS_N . This space displays a rhomboidal like truncation in the range $2N \leq n \leq 3N$. In terms of approximation power, this space seems more promising than the space $\mathcal{Y}'_{\text{SVD}}$. This is particularly true regarding the inclusion of a SH Legendre subspace as large as possible in the approximation space.

5.4. Interpolation test cases. We interpolate the following set of test functions on the sphere \mathbb{S}^2 :

$$\begin{aligned}
f_1(x, y, z) &= 1 + x + y^2 + yx^2 + x^4 + y^5 + x^2y^2z^2, \\
f_2(x, y, z) &= \frac{3}{4} \exp \left[-\frac{(9x-2)^2}{4} - \frac{(9y-2)^2}{4} - \frac{(9z-2)^2}{4} \right], \\
&\quad + \frac{3}{4} \exp \left[-\frac{(9x+1)^2}{49} - \frac{9y+1}{10} - \frac{9z+1}{10} \right], \\
&\quad + \frac{1}{2} \exp \left[-\frac{(9x-7)^2}{4} - \frac{(9y-3)^2}{4} - \frac{(9z-5)^2}{4} \right], \\
&\quad - \frac{1}{5} \exp \left[-(9x-4)^2 - (9y-7)^2 - (9z-5)^2 \right], \\
f_3(x, y, z) &= \frac{1}{9} [1 + \tanh(-9x - 9y + 9z)], \\
f_4(x, y, z) &= \frac{1}{9} [1 + \text{sign}(-9x - 9y + 9z)].
\end{aligned}$$

The function f_1 is polynomial and $f_1 \in \oplus_{n \leq 6} Y_n$. The functions f_2 and f_3 are regular and they have many SH components in their expansion (51). The function f_4 is discontinuous. In Fig. 5, the interpolation errors with $N = 2$ and $N = 4$ for this set of functions is displayed. Furthermore, we display in Fig. 6 the uniform error and the root mean squared error (RMSE) on CS_M , with $M = 65$; they are defined by

$$\begin{cases} e_\infty(N, f_i) \triangleq \|f_i|_{\text{CS}_M} - \mathcal{I}_N f_i|_{\text{CS}_M}\|_\infty = \max_{\mathbf{x} \in \text{CS}_M} |f_i(\mathbf{x}) - (\mathcal{I}_N f_i)(\mathbf{x})|, \\ e_2(N, f_i) \triangleq \frac{1}{(6M^2+2)^{1/2}} \|f_i|_{\text{CS}_M} - \mathcal{I}_N f_i|_{\text{CS}_M}\|_2 \\ \quad = \left(\frac{1}{6M^2+2} \sum_{\mathbf{x} \in \text{CS}_M} |f_i(\mathbf{x}) - (\mathcal{I}_N f_i)(\mathbf{x})|^2 \right)^{1/2}, \end{cases} \quad (58)$$

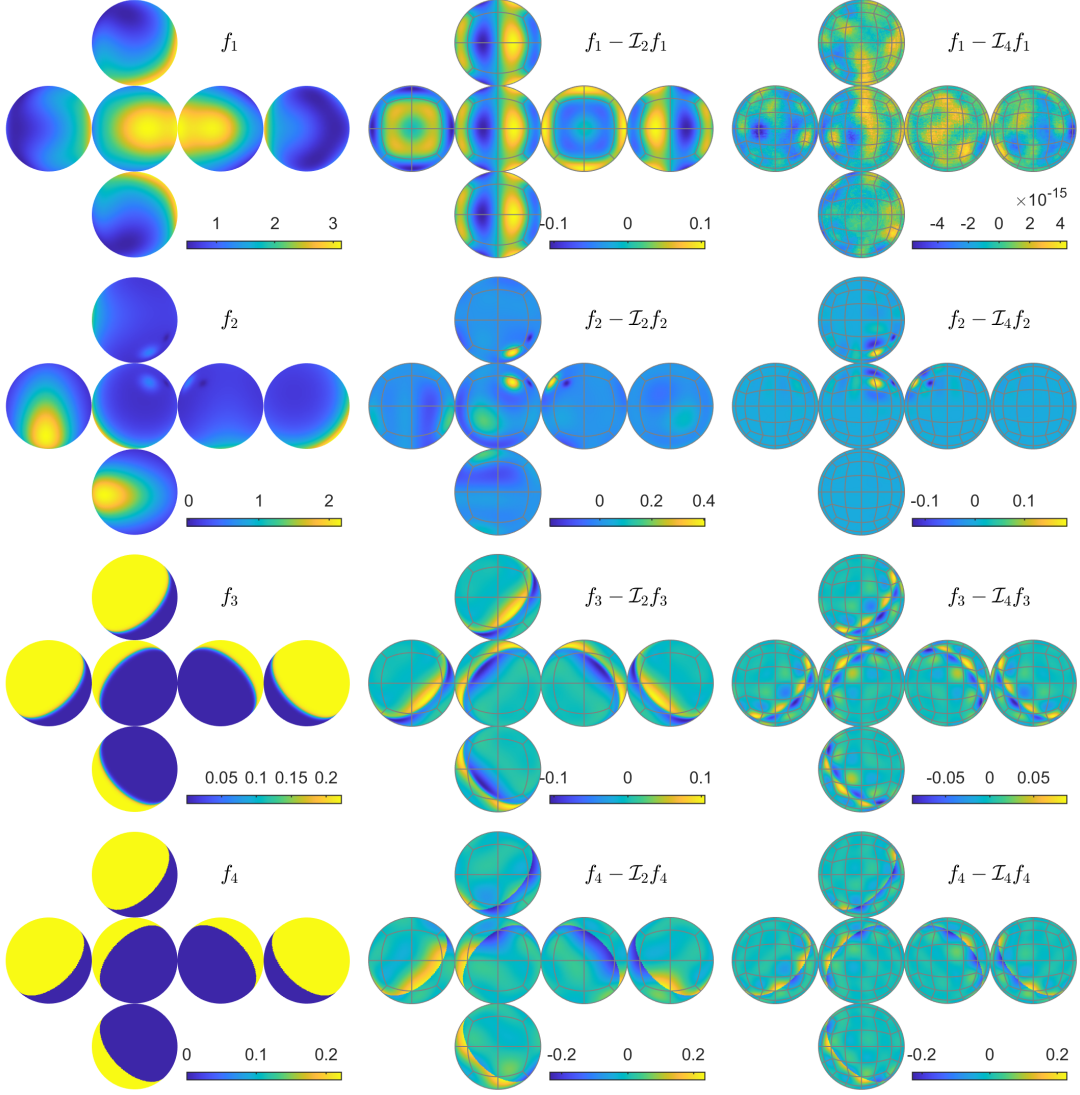


FIGURE 5. Interpolation of the test functions f_1 , f_2 , f_3 and f_4 . Left column: the four test functions. Middle column: interpolation error on CS_2 . Right column: interpolation error on CS_4 .

where $\mathcal{I}_N f \in \mathcal{Y}'_{3N}$ stands for the interpolating function of $[f(\mathbf{x}_j)]$. For N large enough, $f_1 \in \mathcal{Y}'_{3N}$, which gives a null error. The smooth function f_2 is interpolated with an error decreasing with N . This is also the case for the function f_3 , with a decreasing rate smaller than the one for f_2 . This reflects the C^p regularity of the functions f_2 and f_3 . Finally, as expected, the discontinuous function f_4 is not well interpolated. The RMSE decreases very slowly, and the uniform error does not decrease.

5.5. Poisson equation on the sphere. Let $g : \mathbf{x} \in \mathbb{S}^2 \mapsto g(\mathbf{x})$ a function defined on the sphere. We consider the null mean Poisson equation on the sphere in the class of regular functions (say C^∞):

$$\begin{cases} \Delta u = g \text{ on } \mathbb{S}^2, \\ \int_{\mathbb{S}^2} u d\sigma = 0. \end{cases} \quad (59)$$

Consider the expansion (51) of g

$$g = \sum_{n \geq 0} \sum_{|m| \leq n} g_{n,m} Y_n^m. \quad (60)$$

Then, using that

$$\Delta Y_n^m = -n(n+1)Y_n^m, \quad (61)$$

the solution of (59) is expressed as

$$g = - \sum_{n \geq 1} \sum_{|m| \leq n} \frac{g_{n,m}}{n(n+1)} Y_n^m. \quad (62)$$

The null mean assumption on u gives that there is no contribution for $n = 0$.

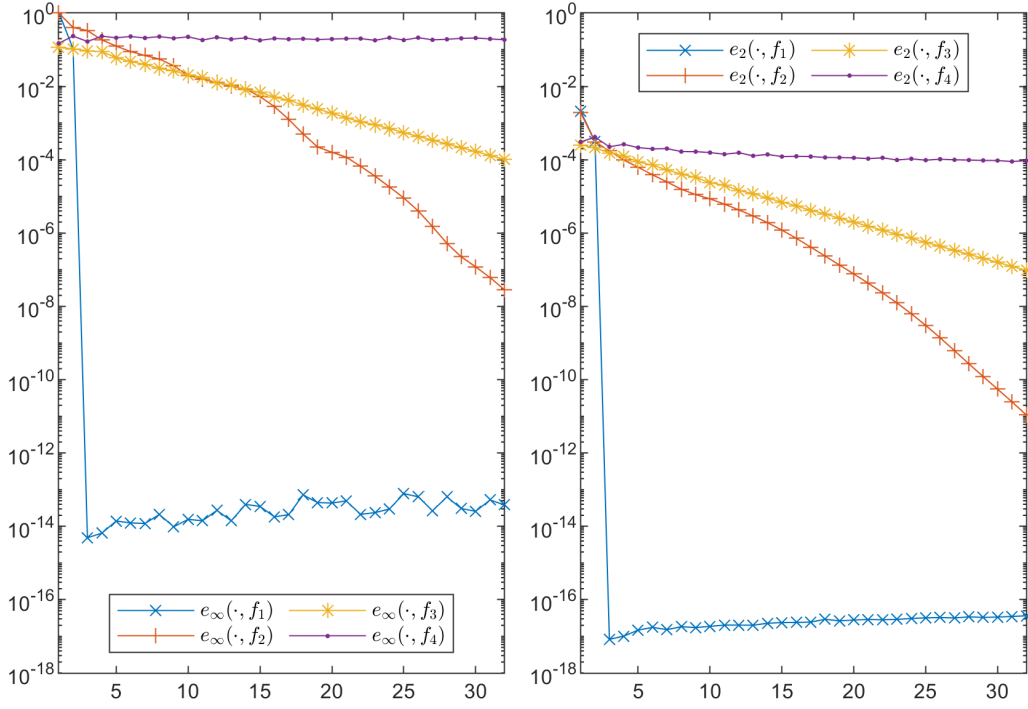


FIGURE 6. Interpolation error of test functions on CS_N , for $1 \leq N \leq 32$. Left: uniform error e_∞ ; right: RMSE e_2 . Each error is evaluated on CS_{65} , and represented in logarithmic scale.

Consider the Cubed-Sphere CS_N . Our numerical scheme to approximate (59) using the space \mathcal{Y}'_{3N} in (48) is to use a pseudospectral approach as follows.

- (1) Define g^* , the restriction of $g(\mathbf{x})$ to CS_N , by

$$g_j^* \triangleq [g(\mathbf{x}_j)], \quad j \in \llbracket 1 : \bar{N} \rrbracket. \quad (63)$$

- (2) Calculate the SH function $g_h(\mathbf{x}) \in \mathcal{Y}'_{3N}$ defined by

$$g_h(\mathbf{x}) \triangleq \sum_{|m| \leq n \leq 3N} \hat{g}_n^m Y_n^m(\mathbf{x}), \quad (64)$$

where the vector $\hat{g} \in \mathbf{R}^{\bar{N}}$ is given by $\hat{g} \triangleq \tilde{U}_{3N}(\mathbf{L}_{3N}^\top)^{-1} \mathbf{V}_{3N}^\top g^*$.

- (3) Define $\hat{u} \in \mathbf{R}^{\bar{N}}$ by $\hat{u} \triangleq \Lambda \hat{g}$ where Λ is the diagonal matrix

$$\Lambda \triangleq \begin{bmatrix} \Lambda^{(0)} & & & \\ & \Lambda^{(1)} & \mathbf{0} & \\ & \mathbf{0} & \ddots & \\ & & & \Lambda^{(3N)} \end{bmatrix} \in \mathbb{R}^{\bar{N} \times \bar{N}}, \quad \text{with } \Lambda^{(0)} \triangleq 0, \quad \Lambda^{(n)} \triangleq -\frac{1}{n(n+1)} \mathbf{I}_{2n+1}, \quad 1 \leq n \leq 3N.$$

- (4) Define $u_h(\mathbf{x})$ by

$$u_h(\mathbf{x}) \triangleq \sum_{|m| \leq n \leq 3N} \hat{u}_n^m Y_n^m(\mathbf{x}). \quad (65)$$

- (5) Evaluate u_h^* , the restriction of $u_h(\mathbf{x})$ to CS_N .

Selecting $\Lambda^{(0)} = 0$ implies that $\int_{\mathbb{S}^2} u_h d\sigma = 0$ at the discrete level. Second, according to Corollary 17, $u_h = u$ in the case where $g \in \mathcal{Y}'_{3N}$.

We consider the test case of [4, 19]. Let $g = g_a + g_b$ be given in longitude-latitude coordinate (λ, θ) where

$$\begin{cases} g_a(\lambda, \theta) = -(m+1)(m+2) \sin(\theta) \cos^m(\theta) \cos(m(\lambda - d_m)), \\ g_b(\lambda, \theta) = m(m+1) \cos^m(\theta) \cos(m(\lambda - e_m)). \end{cases} \quad (66)$$

The exact solution is $u = u_a + u_b$ with

$$\begin{cases} u_a(\lambda, \theta) = \begin{cases} -\sin(\theta) \cos^m(\theta) \cos(m(\lambda - d_m)), & \text{if } m > 0, \\ -\sin(\theta) - 1, & \text{if } m = 0, \end{cases} \\ u_b(\lambda, \theta) = \cos^m(\theta) \cos(m(\lambda - e_m)). \end{cases} \quad (67)$$

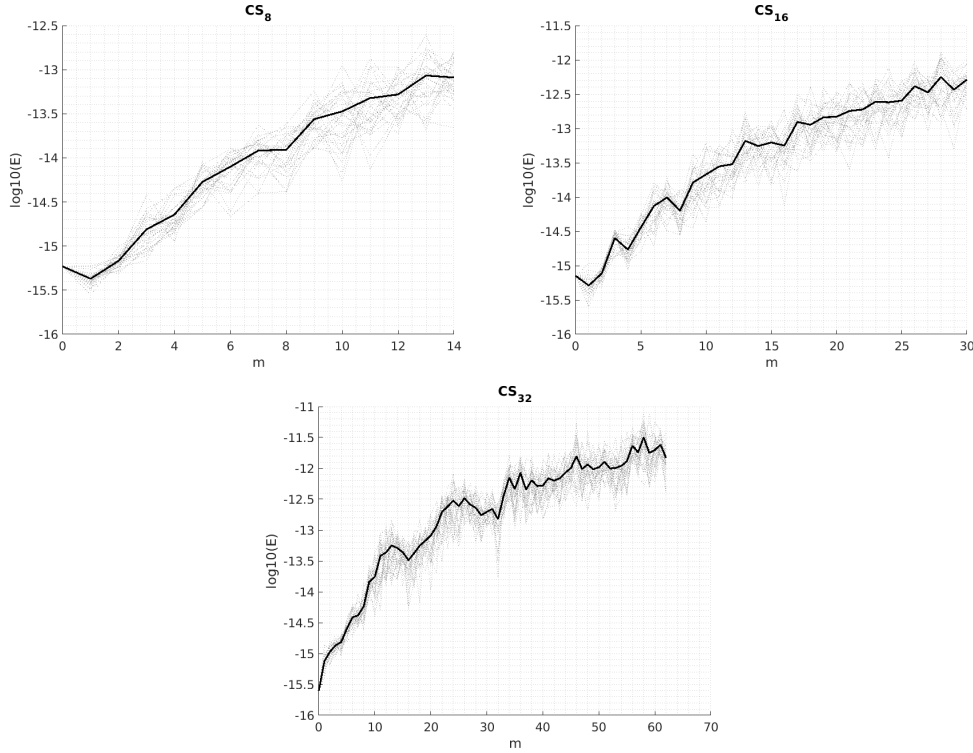


FIGURE 7. Poisson equation solver error on CS_N for $N \in \{8, 16, 32\}$. The relative error is plotted related to the value m for 30 random values e_m and d_m in $[0, 2\pi]$.

	$m = 2N - 1$	$m = 2N$	$m = 2N + 1$
$N = 8$	4.53×10^{-9}	3.25×10^{-4}	2.74×10^{-1}
$N = 16$	3.31×10^{-13}	2.96×10^{-6}	1.31×10^{-1}
$N = 32$	1.91×10^{-12}	1.33×10^{-9}	6.40×10^{-2}

TABLE 5. Poisson equation error on CS_N for $N \in \{8, 16, 32\}$. The relative error E in (68) is related to the value m . It is averaged over 30 random values e_m and d_m in $[0, 2\pi]$.

In the sequel, the values e_m and d_m are phase angles in $[0, 2\pi]$, picked at random. The accuracy is evaluated by

$$E = \left(\frac{\sum_{\mathbf{x}_j \in CS_N} |u_h(\mathbf{x}_j) - u(\mathbf{x}_j)|^2}{\sum_{\mathbf{x}_j \in CS_N} |u(\mathbf{x}_j)|^2} \right)^{1/2}. \quad (68)$$

This evaluation is repeated for 30 random values of e_m and d_m in $[0, 2\pi]$. Fig 7 reports the mean value of $\log_{10}(E)$ in function of m . Three Cubed Spheres are considered, CS_8 , CS_{16} and CS_{32} . For a given grid CS_N , the error E increases with m , which is expected, due to the cut-off in resolution of the grid. The magnitude of the error E is similar to the one reported in [4] which uses a standard pseudospectral solver with a lon-lat grid. Here, there is no loss in accuracy, despite that the function (67) is expressed in lon-lat coordinates. The truncation reported in Section 5.2 is analyzed as follows. In Table 5 the error E is reported for $m \in \{2N - 1, 2N, 2N + 1\}$. Consider for example CS_{16} . For $m = 2N - 1$, the error is of the order of 10^{-13} . For $m = 2N$, the error is augmented by a factor of 10^5 , which gives $E \simeq 10^{-6}$. Finally, another augmentation by the same factor of 10^5 occurs again leading to $E \simeq 10^{-1}$ for $m = 2N + 1$. This corresponds to an undersampling of the function g along the equator.

6. CONCLUSION

In this study, a methodology to associate a Spherical Harmonics subspace to the Cubed Sphere CS_N has been introduced. The particular subspace considered in Section 4 is based on a specific Column Echelon factorization of the Vandermonde matrix. This space seems promising in terms of approximation power. As seen in Section 5.2, it compares favourably to alternatives factorizations, such as the SVD.

This work took its origin in the numerical observation of the rank increment property stated in Claim 18. A proof of this claim, which is not available at time, is an objective of further studies. Using the new

interpolation procedure to various contexts is also a future goal. First, spherical quadrature rules will be addressed elsewhere. Another issue is the symmetry properties of the interpolation space. This includes studying the invariance under the action of the group of the sphere, has to be undertaken, in the line of [2]. Computational issues clearly require further analysis. Preliminary observations are presented in Appendix A (condition number of the Vandermonde matrix and run time to evaluate the SH basis).

Finally, an important goal is the application of this new framework to PDE's in meteorology, in the spirit of the approach in Section 5.5.

APPENDIX A. COMPUTATIONAL ISSUES

We report in Table 6, some data related to the computation of the Vandermonde matrix \mathbf{A}_{3N} in (22) and of the lower triangular matrix \mathbf{L}_{3N} in (38). A condition number of magnitude 1 – 10 is observed in both

N	1	2	4	8	16	32
$\bar{N} = 6N^2 + 2$	8	26	98	386	1538	6146
cond \mathbf{A}_{3N}	2	2	2.1	2	2.5	6.1
cond \mathbf{L}_{3N}	2	2.2	2.1	2.3	3	7.4
CPU time (s)	8.8e-03	1.7e-03	6.7e-03	1.1e-01	4.7e+00	3.0e+02

TABLE 6. For the Cubed Sphere CS_N , the condition number of the matrices \mathbf{A}_{3N} and \mathbf{L}_{3N} are similar, (see Claim 18 and Corollary 16). The reported CPU time in secs. corresponds to a matlab code performed using a CPU Intel i9-9880H@2.30 GHz.

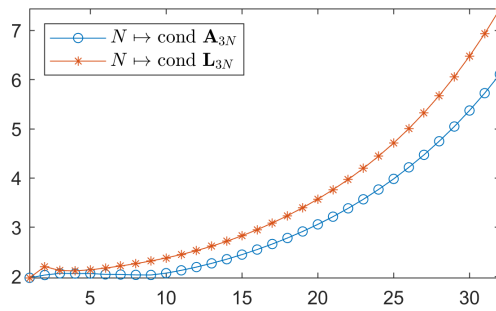


FIGURE 8. Condition number of the matrices \mathbf{A}_{3N} and \mathbf{L}_{3N} for $1 \leq N \leq 32$.

cases; for example, for $N = 32$, the number of grid points is $\bar{N} = 6146$, and $\text{cond } \mathbf{L}_{3N} = 7.4$. As a result, at moderate values of \bar{N} , we expect an accurate evaluation of the interpolating functions. The condition numbers of \mathbf{A}_{3N} and \mathbf{L}_{3N} in function of N are similar. This indicates that the factorization (39) practically preserves the condition number of the full VDM matrix \mathbf{A}_{3N} .

In last line of Table 6, the reported CPU time corresponds to the computation of the matrix \mathbf{L}_{3N} , of the full basis U_k of Y_k , $0 \leq k \leq 3N$, and of the orthogonal matrix \mathbf{V}_{3N} . It also includes assembling the matrices A_k , $k \leq 3N$. For each value $N = 1, 2, 4, 8, 16, 32$, the computations are repeated five times and the reported CPU time is the average.

APPENDIX B. REPRESENTATION OF THE BASIS FUNCTIONS FOR $N = 2$

For completeness, we display the computed basis for $N = 2$. Fig. 9 shows the basis of the subspace \mathcal{Y}'_6 and Fig. 10 displays the basis of the orthogonal set $(\mathcal{Y}'_6)^\perp$. For each basis function u , the convention is the following: we plot u on the sphere, and we draw the CS_2 mesh; then six views of this sphere are displayed, corresponding to the six panels of the cubed sphere.

REFERENCES

- [1] K. Atkinson and W. Han. *Spherical Harmonics and Approximations on the Unit Sphere: an introduction*. Number 2044 in Lect. Notes. Math. Springer-Verlag, 2012.
- [2] J.-B. Bellet. Symmetry group of the equiangular cubed sphere. *hal-03071135*, 2020.
- [3] M. Brachet and J.-P. Croisille. Spherical shallow water simulation by a cubed sphere finite difference solver. *Quat. J. Roy. Met. Soc.*, 147(735):786–800, 2021.
- [4] H.-B. Cheong. Double Fourier series on a sphere: applications to elliptic and vorticity equations. *J. Comp. Phys.*, 157:327–349, 2000.

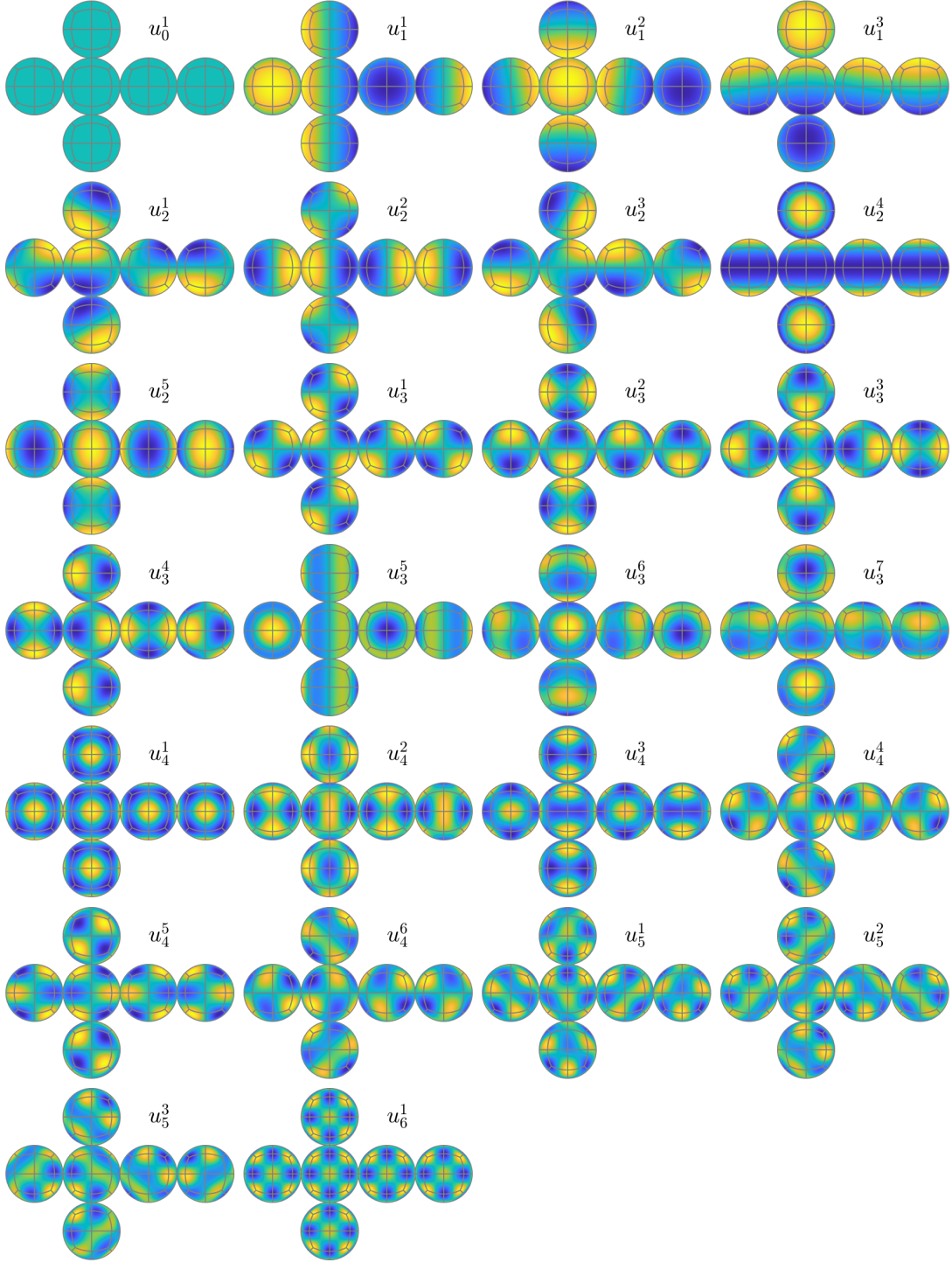


FIGURE 9. Orthonormal basis $u_n^i \in Y_n' \subset Y_n$, $1 \leq i \leq g_n$, $0 \leq n \leq 3N$, of the unisolvent set $\mathcal{Y}_{3N}' = \oplus_{0 \leq n \leq 3N} Y_n'$. The Cubed Sphere is CS_2 , ($N = 2$).

- [5] W. D. Collins et al. Description of the NCAR Community Atmosphere Model (CAM 3.0). NCAR Technical Note TN-464+STR, NCAR, 2004.
- [6] R. Daley and Y. Bourassa. Rhomboidal versus triangular spherical harmonic truncation:some verification statistics. *Atmosphere-Ocean*, 16(2):187–196, 2010.
- [7] G. Golub and C. Van Loan. *Matrix Computations*. John Hopkins University Press, 3-rd edition, 1996.
- [8] D. Gottlieb and S. Orszag. *Numerical Analysis of Spectral Methods: Theory and Applications*. SIAM, 1977.
- [9] M. N. Jones. *Spherical Harmonics and Tensors for classical field theory*. Research Studies Press, 1985.
- [10] S. Kunis, H. Möller, and U. von der Ohe. Prony's method on the sphere. *SMAI J. of Comp. Math.*, S5:87–97, 2019.
- [11] B. Machenhauer. The spectral method. In *Numerical methods used in atmospheric models*. World meteorological organisation, Geneva, Switzerland, 1979.
- [12] R. Nair, S. J. Thomas, and R. D. Loft. A discontinuous Galerkin transport scheme on the cubed sphere. *Month Weath. Rev.*, 133(4):814–828, 04 2005.
- [13] R. Purser and M. Rančić. Smooth quasi-homogeneous gridding of the sphere. *J. Comp. Phys.*, 124:637–647, 1998.

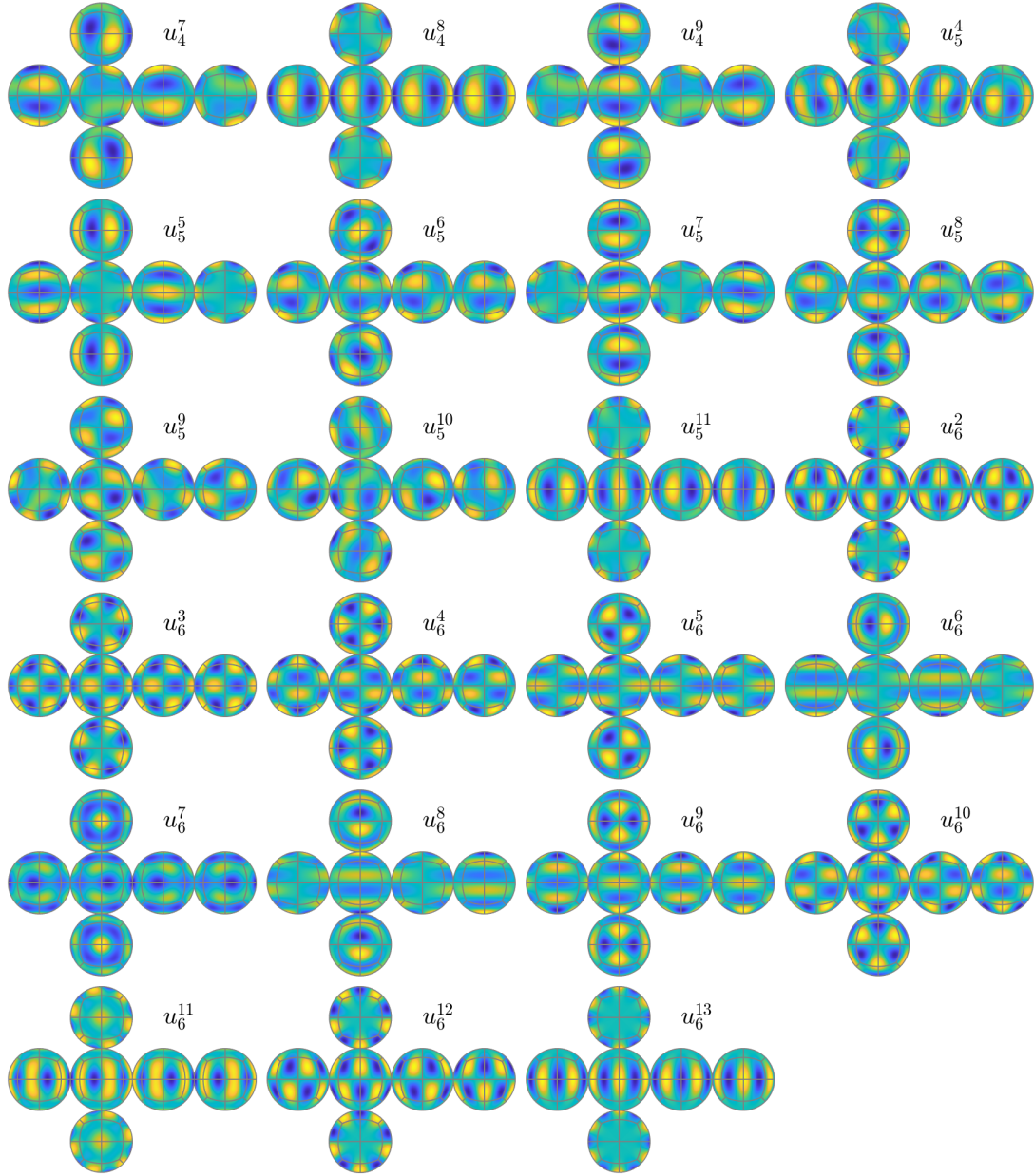


FIGURE 10. Orthonormal basis $u_n^i \in Y_n''$, $g_n + 1 \leq i \leq 2n + 1$, $2N \leq n \leq 3N$, of the orthogonal supplementary $(\mathcal{Y}_{3N}')^\perp = \oplus_{2N \leq n \leq 3N} Y_n''$. The Cubed Sphere is CS_2 , ($N = 2$).

- [14] M. Rančić, R. Purser, and F. Mesinger. A global shallow-water model using an expanded spherical cube: Gnomonic versus conformal coordinates. *Quart. J. Roy. Met. Soc.*, 122:959–982, 1996.
- [15] C. Ronchi, R. Iacono, and P. S. Paolucci. The Cubed Sphere: A new method for the solution of partial differential equations in spherical geometry. *J. Comp. Phys.*, 124:93–114, 1996.
- [16] R. Sadourny. Conservative finite-difference approximations of the primitive equations on quasi-uniform spherical grids. *Mon. Wea. Rev.*, 100:136–144, 1972.
- [17] S. J. Thomas, J. Dennis, H. Tufo, and P. F. Fisher. A Schwarz preconditionner for the cubed sphere. *SIAM J. Sci. Comp.*, 25(2):442–453, 2003.
- [18] P. A. Ullrich, C. Jablonowski, and B. van Leer. High order finite-volume methods for the shallow-water equations on the sphere. *J. Comp. Phys.*, 229:6104–6134, 2010.
- [19] Y. Yee. Solution of Poisson's equation on a sphere by truncated double Fourier series. *Mon. Weath. Rev.*, 109:501–501, 1981.

[†] UNIVERSITÉ DE LORRAINE, CNRS, IECL, F-57000 METZ, FRANCE

Email address: jean-baptiste.bellet@univ-lorraine.fr, jean-pierre.croisille@univ-lorraine.fr

[‡] UNIVERSITÉ DE POITIERS, CNRS, LMA, F-86000 POITIERS, FRANCE

Email address: matthieu.brachet@math.univ-poitiers.fr